Investigation of Water Evaporation and Salt Precipitation at CO_2 Geological Storage Condition

Zhe Wang[1], Panrui Yang[1], Huirong Guo[1]†, Qian Zhou[1], Linlin Lin[2] and Min Yuan[1]

[1]School of Environmental Studies, China University of Geosciences, 430074, Wuhan, China

[2]Shandong Provincial Lunan Geology and Exploration Institute（Shandong Provincial Bureau of Geology and Mineral Resources NO.2 Geological Brigade）, 272100, Yanzhou, China

Corresponding author: Huirong Guo (hrguo@cug.edu.cn)

Key Points:

- 22 diffusion coefficient data are obtained at 10-50 MPa and 353.15-433.15 K.
- Diffusion coefficient is used to predict when salt precipitation occurs at a site of Alberta Basin.
- Salt precipitation for CO_2 dry-out was observed in a capillary tube and a micromodel respectively.

Abstract

CO_2 geological storage is a promising method to dispose excess CO_2 in the atmosphere, and the existence of brine in deep saline aquifer and below oil reservoir may lead to salt precipitation in pore space for dry-out formation. Water diffusion coefficient is helpful to evaluate salt precipitation. However, limited previous data can't satisfy the need of CO_2 geological storage. Raman quantitative spectroscopy is used to observe water diffusion in CO_2 in a high-pressure capillary cell and corresponding diffusion coefficients are obtained at 10-50 MPa and 353.15-433.15 K. Diffusion coefficient is temperature and pressure dependent, and also increases linearly with the reciprocal of CO_2 density. Free volume theory and PC-SAFT EOS are utilized to establish a thermodynamic model for water diffusion in CO_2, and it predicts diffusion coefficient accurately at 10-50 MPa and 353.15-433.15 K. Besides, diffusion coefficient is used to evaluate when salt precipitation occurs and salt precipitation process is observed in a one-dimensional capillary tube and a two-dimensional micromodel respectively.

1 Introduction

CO_2 concentration increases clearly in the atmosphere for huge energy demand (Guyant et al., 2015; Roels et al., 2014), and for now, injecting CO_2 into geological formations is a promising method to mitigate CO_2 emission, including saline aquifer, producing/depleted oil field and coal bed (Bai et al., 2018; Miri et al., 2015; Muller et al., 2009). For saline aquifer and oil filed, dissolution is a major mechanism, including CO_2 dissolution in brine and oil (Guo et al., 2016; Han & Mcpherson, 2009) and when CO_2 contacts brine, CO_2 plume displaces brine and interphase mass transfer exists between CO_2 and brine (Pruess & Müller, 2009) which means dry CO_2 dissolves into water and also dries out water at the same time (Ott et al., 2015). CO_2 evaporating water increases brine concentration, and when salt concentration reaching salt solubility, salt precipitation will occur (Muller et al., 2009) which has a obvious effect on CO_2 injectivity and storage safety (Gaus, 2010). Generally, salt precipitation near injection wells does impair injectivity (Jeddizahed & Rostami, 2016; Muller et al., 2009) while that near reservoir covers is beneficial for storage safety (Gaus, 2010). Water evaporation rate, in other words, diffusion coefficient in CO_2 is desired for evaluating salt precipitation and CO_2 geological storage.

There are limited studies about water diffusion in CO_2 in previous study. Xu et al. (2003) utilized NMR to observe the sample cells to obtain the water diffusion coefficient at 283.15 K, 298.15 K and 308.15 K and 13-30 MPa. Espinoza and Santamarina (2010) observed the instantaneous droplet volume and surface area to evaluate the water diffusion coefficient in CO_2 at the pressure of 7.8-14.4 MPa and temperature of 296.5±1.5 K. Schwertz and Brow (1951) observed the alteration of liquid level in an isothermal atmosphere of CO_2 and measured the water diffusion coefficient at 1 bar and temperature of 307.45 K, 328.55 K and 352.35 K. According to Fig. 1, most previous experimental data are out of CO_2 supercritical condition which is the major condition for CO_2 in geological storage. These experimental data are not suitable for the reservoir condition of CO_2 geological storage.

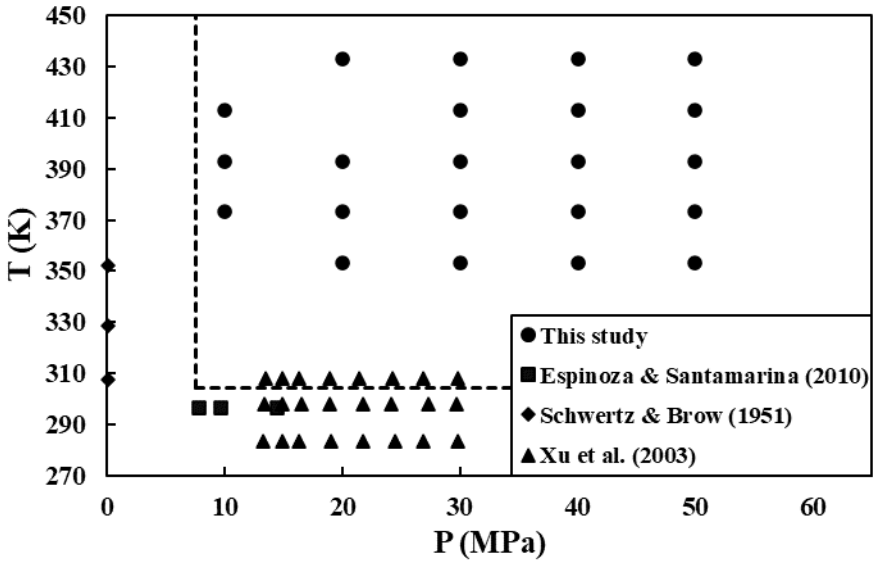

Figure 1. Pressure and temperature in previous study and this study (Espinoza & Santamarina, 2010; Schwertz & Brow, 1951; Xu et al., 2003). Dashed line: pressure and temperature of CO_2 supercritical condition.

Partly like the previous study (Lu et al., 2013), Raman quantitative is used to obtain water concentration profile in CO_2 in this study. Differently, there is a steady-state and semi-infinite diffusion in gas phase, and Fick's first law is suitable to explain the diffusion phenomenon. According to Fick's First Law, diffusion flux and concentration gradient need to be measured to calculate diffusion coefficient, and for steady-state diffusion, the flux and concentration gradient are constant. Water diffusion process is observed at 10-50 MPa and 353.15-433.15 K, and based on the concentration profiles and water change rate, corresponding diffusion coefficients are obtained. Based on free volume theory and SAFT EOS, a thermodynamic model for water diffusion was established and is able to predict water diffusion coefficient accurately at 10-50 MPa and 353.15-433.15 K. With the help of this model, the calculated data is used to predict when salt precipitation occurs at Alberta Basin site 11. What's more, salt precipitation is investigated in a one-dimensional capillary tube and two-dimensional micromodel to observe the salt crystal variation and distribution in porous media.

2 Materials and Methods

2.1 Sample preparation and spectra collection

Procedures of sample preparation and material are same as sample loading of (Lu et al., 2013), but procedures of Raman spectra collection and diffusion coefficient calculation are different.

After sample loading, the sample is kept at the experimental P-T condition for 1-2 days. When the concentration gradient and interface change rate are constant, there reaches a steady-state diffusion in the gas phase which accords with Fick's first law. Five certain spots at a constant distance are chosen to collect Raman spectra to obtain water concentration profile in gas

phase (Fig. 2), and at the same time, alteration of interface with time is recorded for calculation of diffusion flux. Positions for spectra should be changed with the changing interface, for the purpose of making distance between interface and positions constant.

For spectra processing, areas of water peak (3600-3680 cm^{-1}) and CO_2 peak (1150-1500 cm^{-1}) are obtained to calculate the ratio of area PAR [$H_2O/(H_2O+CO_2)$]. Raman quantitative factors have been measured to calculate water concentration in our previous study (Wang et al., 2018).

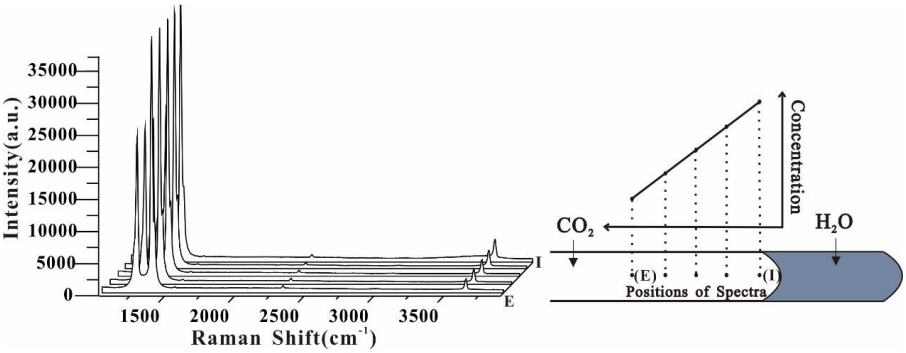

Figure 2. Spectra of diffusion about water in CO_2. From the interface to the end, the area of water decreases linearly. It indicates concentration of water in CO_2 decreases linearly, and it comes to a steady-state diffusion.

2.2 Calculation of water diffusion coefficient

Fick's first law is

$$J = -D\frac{dC}{dl} \qquad (1)$$

J is diffusion flux; C is concentration of solute; l is distance; D is diffusion coefficient.

Diffusion flux means the velocity of water decreasing. Thus:

$$\frac{\Delta L \times A}{V_m^L} = D \times \frac{\Delta C}{\Delta l} \times \Delta t \times A \qquad (2)$$

ΔL is the alteration of water length, m; A is the area of tube section, m^2; V_m^L is mole volume of water, cm^3/mol; Δt is the alteration of time, s; D is diffusion coefficient, m^2/s; C is concentration of water in carbon dioxide, mol/m^3; Δl is the alteration of distance in different observation positions, m.

Raman quantitative factors (Wang et al., 2018) and PAR are used to calculate the concentration of water in CO_2.

$$C = \frac{x_{H_2O}}{(1-x_{H_2O}) \times V_m^G} \qquad (3)$$

Then

$$\Delta C = C_2 - C_1 = \frac{x_2}{(1-x_2) \times V_m^G} - \frac{x_1}{(1-x_1) \times V_m^G} \qquad (4)$$

According to Fick's first law, the equation is written as

$$\frac{\Delta L}{\Delta t} = \frac{\frac{x_1}{(1-x_1)} - \frac{x_2}{(1-x_2)}}{\Delta l} \times D \times \frac{V_m^L}{V_m^G} \quad (5)$$

Thus, the concentration gradient in gas phase is:

$$K_1 = \frac{\frac{x_1}{(1-x_1)} - \frac{x_2}{(1-x_2)}}{\Delta l} \quad (6)$$

In the study, the diffusion flux of water is expressed as the variation of interface, which is:

$$K_2 = \frac{\Delta L}{\Delta t} \quad (7)$$

According to (5), (6) and (7), diffusion coefficient is:

$$D = \frac{K_2 V_m^G}{K_1 V_m^L} \quad (8)$$

2.3 Observation of salt precipitation

Salt precipitation is observed in a capillary tube as a single pore and a micromodel as a two dimensional porous medium. Load the brine into the capillary tube and micromodel. Evacuate the air and inject into CO_2, and maintain the pressure and temperature using the heating-cooling stage and pressure pump. Observe the salt precipitation process until the all water is evaporated.

3 Results

3.1 Diffusion observation

In this study, there is a steady-state diffusion for water in CO_2. Because CO_2 concentration in water reaches solubility, no more CO_2 dissolves in water 1-2 days later (Lu et al., 2013), and the variation of water volume is completely caused by water dissolving into CO_2. Interface changes with time linearly which means water volume also decreases with time linearly (Fig. 3a) and diffusion flux is constant. Besides, according to the measured water concentration profiles, concentration decreases linearly with distance away from the interface, and fitted concentration gradient is generally constant for every round (Fig. 3b). Moreover, water concentration gradient in CO_2 and interface change rate are relevant to water solubility in CO_2 (Wang et al., 2018) (Fig. 4). The relationship can be used to calculate concentration gradient and diffusion flux for CO_2 dry-out effect.

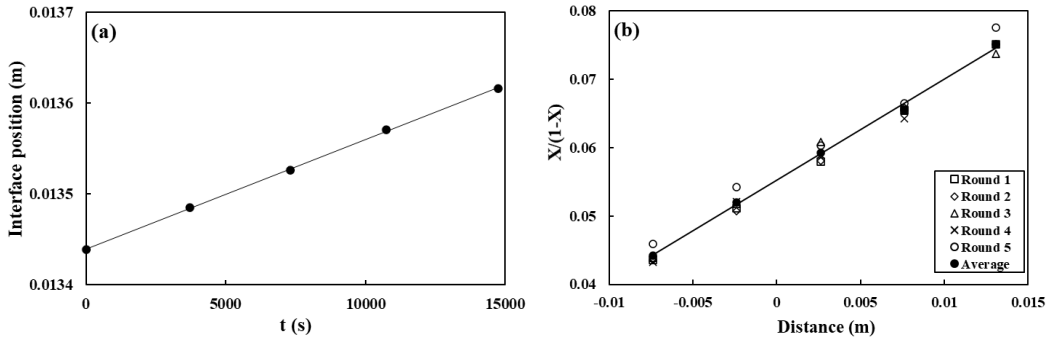

Figure 3. Diffusion observation at 40 MPa, 413.15 K. (a) Interface changes with time; (b) Water concentration profiles in CO_2.

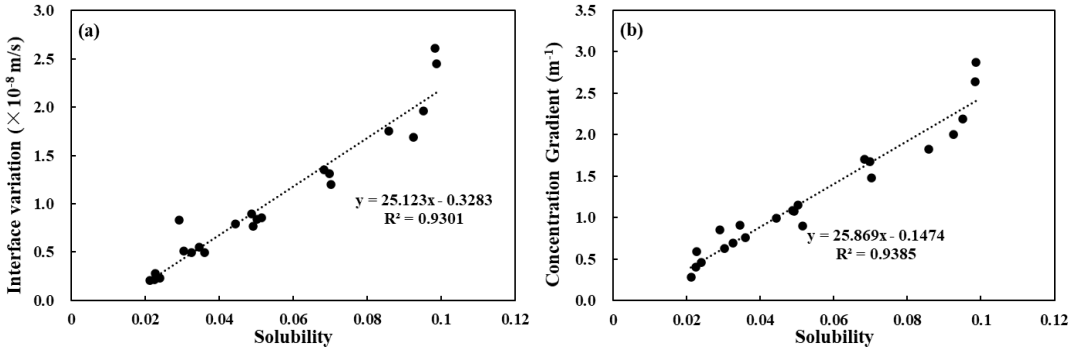

Figure 4. (a) The relationship between interface change rate (representing diffusion flux, K_2) and water solubility in CO_2; (b) The relationship between water concentration gradient in CO_2 (K_1) and water solubility in CO_2 (Wang et al., 2018).

3.2 Calculated diffusion coefficients

By observing the process of the diffusion, water diffusion coefficients in CO_2 were obtained from 10 to 50 MPa and 353.15 to 433.15 K (Table 1).

Table 1. Calculated water diffusion coefficient in carbon dioxide (10^{-8} m^2/s).

T(K)	10 MPa	20 MPa	30 MPa	40 MPa	50 MPa
353		3.02	1.76	1.37	1.41
373	12.13	3.96	2.55	1.91	1.89
393	13.18	4.60	3.29	2.41	2.26
413	14.41		3.46	2.96	2.60
433		7.18	4.12	3.50	2.90

According to calculated results, there's a certain relationship between diffusion coefficient and temperature. The result indicates that at 10 to 50 MPa and 353.15 to 433.15 K, the diffusion coefficient increases linearly with temperature at the same pressure and the slope decreases with increasing pressure (Fig. 5a). Besides, diffusion coefficient decreases obviously with the increasing pressure at the same temperature (Fig. 5b). At low pressure, pressure affects diffusion coefficient more than temperature. Effect of pressure can not be neglected which is different from CO_2 diffusion in water (Lu et al., 2013).

Diffusion coefficient is also affected by the density of solvent, and with density increasing, diffusion coefficient decreases (Yang et al., 2000). Comparing diffusion coefficient in this study and CO_2 density, there's a linear relationship between diffusion coefficient and the reciprocal of CO_2 density (Fig. 5c). It is significant to use CO_2 density to calculate diffusion coefficient in different temperature and pressure. Comparing between calculation from density and experiment measurement, the average standard deviation is 3.71%.

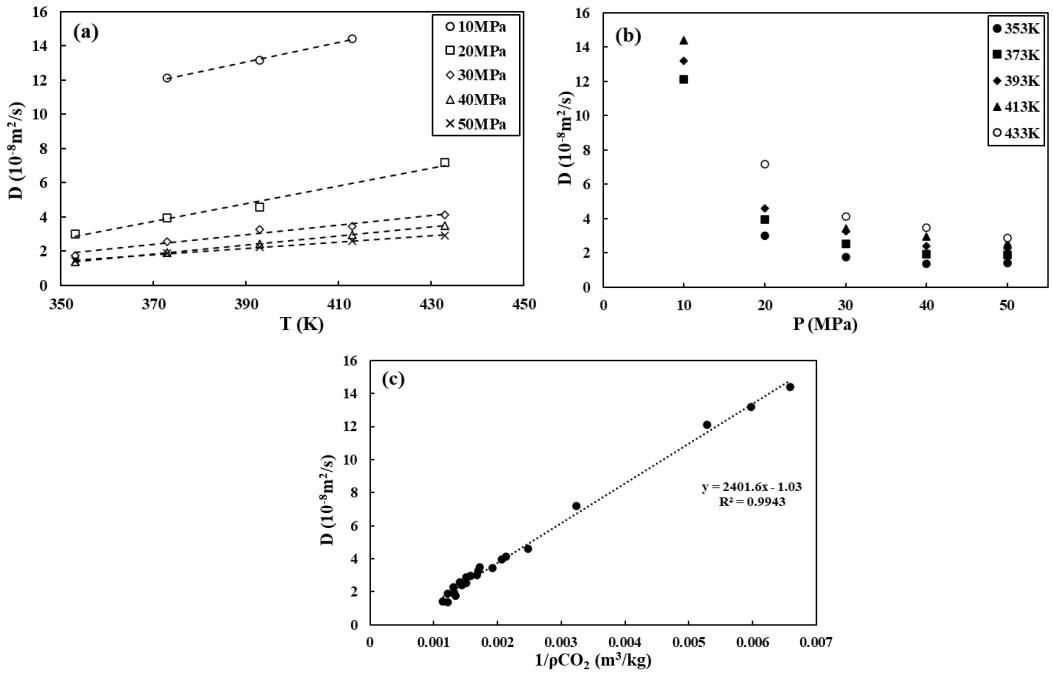

Figure 5. The relationship between thermodynamic parameters and water diffusion coefficient in CO_2. (a) Temperature; (b) Pressure; (c) CO_2 density.

3.3 Comparison with previous study

Temperature and pressure of previous study (Espinoza & Santamarina, 2010; Xu et al., 2003) are different from those in this study and experimental data can't be compared directly through pressure and temperature. According to the relationship between diffusion coefficient and CO_2 density, it's feasible to replace temperature and pressure with density to compare with previous experimental data. Fig. 6 shows data of Xu et al. (2003) are similar with this study. Comparing the function of diffusion coefficient with density and Xu et al. (2003), the average standard deviation is 8.28%.

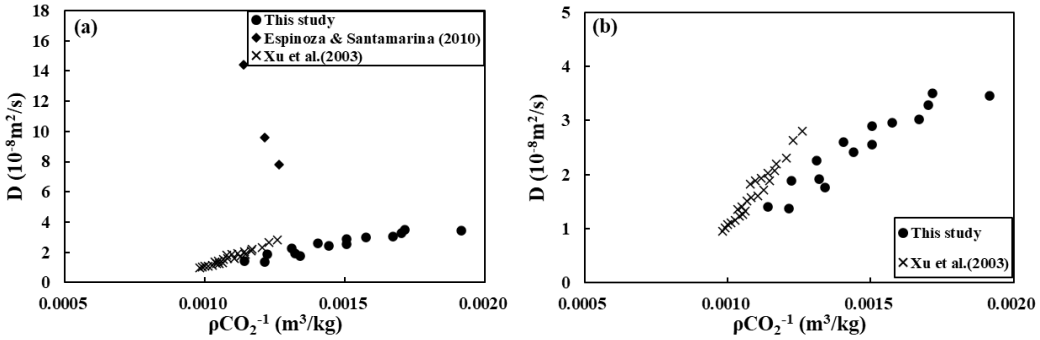

Figure 6. Comparison with previous experimental data.

3.4 Diffusion model of water in CO_2

Based on a generalized free-volume model, self-diffusion coefficient can be expressed as (Liu et al., 2002):

$$D_{self} = A_D\sqrt{\frac{kT}{3.14M}}\left(V^* + \frac{V_f}{\gamma}\right)exp\left(-\frac{\gamma V^*}{V_f} - 2\alpha\varphi\right) \quad (9)$$

D_{self} is the self-diffusion coefficient for fluid; A_D is a constant; k is Boltzmann constant; M is the molar mass; R is the gas constant; V^* is the molar critical free volume; γ is a numerical factor; V_f is the free volume; φ is the mean potential energy.

According the EOS, the compressibility factor (Z) is expressed by attractive (Z^a) and repulsive (Z^r) compressibility. According to the GvdW theory, the Z is expressed as (Liu et al., 2002):

$$Z = V(\frac{\partial lnv_f}{\partial V})_{T,N} - \frac{V}{2kT}\left(\frac{\partial\varphi}{\partial V}\right)_{T,N} = Z^r + Z^a \quad (10)$$

Combining PC-SAFT, Eq. 10 is written as:

$$Z = mV(\frac{\partial lnv_f}{\partial V})_{T,N} - \frac{V}{2kT}\left(\frac{\partial\varphi}{\partial V}\right)_{T,N} = mZ^r + Z^a \quad (11)$$

The free volume theory is correlated with equation of state to evaluate the self-diffusion coefficient of fluid. The PC-SAFT EOS is introduced to correlate the free volume theory. According to the PC-SAFT EOS, the PC-SAFT equation is expressed by the residual Helmholtz energy (Gross & Sadowski, 2001).

$$a^{res} = a^{hs} + a^{chain} + a^{dis} + a^{sas} \quad (12)$$

a^{res}, a^{hs}, a^{chain}, a^{dis}, a^{sas} are the residual, hard-sphere term, chain term, dispersive term and association interaction term hemholtz energy, respectively.

$$a^{res} = -mln\left(\frac{V_f}{V}\right) - \frac{\varphi}{2} \quad (13)$$

$$mln\left(\frac{V_f}{V}\right) = m\frac{3\eta^2-4\eta}{(1-\eta)^2} = -a^{hs} \quad (14)$$

m is the segment parameter in PC-SAFT; η is the reduced density in PC-SAFT (Liu et al., 2002).

Based on the previous study about water and CO_2 self-diffusion coefficients (Kazimierz Krynicki et al., 1978; Robb & Drickamer, 1951; Woolf & Dyo, 1974), modified parameters are listed at Table 2.

Table 2. Parameters for CO_2 and water self-diffusion models.

	CO_2	Water
α	0.116699	0.138828
A_D	0.843494	117.728

The self-diffusion model is extended to calculate the mutual diffusion coefficient. Mutual diffusion coefficient is mainly determined by solvent property. When water dissolves into CO_2, water molecule replaces CO_2 molecule and can be regarded as CO_2 molecule, and the model of water diffusion in CO_2 is based on CO_2 self-diffusion model. But the activation energy of water is different from that of CO_2. The water diffusion coefficient can be obtained as:

$$D_{12} = A_{D,1}\sqrt{\frac{kT}{3.14M_{12}}}\left(V^* + \frac{V_1^f}{\gamma}\right)exp\left(-\frac{\gamma V^*}{V_1^f} - \varphi_{12}\right) \quad (15)$$

$$M_{12} = \frac{2M_1M_2}{M_1+M_2} \quad (16)$$

$$\varphi_{12} = \frac{2\left(-m_1\ln\left(\frac{V_1^f}{V_1}\right)\alpha_{12} - \beta\alpha_2^{res}\right)}{T^*} \quad (17)$$

$$T^* = \frac{T}{\frac{\varepsilon_{12}}{k}} \quad (18)$$

$$\frac{\varepsilon_{12}}{k} = (1-a_1)\sqrt{\frac{\varepsilon_1\varepsilon_2}{k^2}} \quad (19)$$

T^* is the reduced temperature of solvent; φ_{12} is the attractive potential energy; ε_1, ε_2 are parameters for CO_2 and water respectively from PC-SAFT.

β is dependent on temperature in the following equation:

$$\beta = c_1 + c_2T^2 \quad (20)$$

Based on experimental data in this study, modified parameters are listed at Table 3.

Table 3. Parameters for model of water diffusion in CO_2.

α_{12}	a_1	c_1	c_2
-0.24687	4.45404	-0.03805	1.28×10^{-6}

Based on the obtained model, the average deviation between calculated data and experimental data is 4.82%, but the average deviation between the model and Xu et al.(2003) is 57.99% (Table 4). This model can predict water diffusion coefficient in CO_2 accurately at 10-50 MPa and 353.15-433.15 K and can't predict that at low pressure and temperature.

Table 4. Relative deviation between the model and experimental data.

This study			Xu et al. (2003)		
P (MPa)	T (K)	Relative Deviation (%)	P (MPa)	T (K)	Relative Deviation (%)
10	373.15	2.65	13.2	283.15	59.86
10	393.15	1.72	14.83	283.15	59.72
10	413.15	1.29	16.26	283.15	59.91
20	353.15	6.69	18.98	283.15	59.24
20	373.15	0.25	21.77	283.15	59.35
20	393.15	9.11	24.49	283.15	59.55
20	433.15	7.85	26.87	283.15	95.86
30	353.15	9.83	29.8	283.15	58.10

30	373.15	0.60	13.33	298.15	57.83
30	393.15	2.97	14.83	298.15	55.63
30	413.15	8.74	16.46	298.15	53.60
30	433.15	3.25	18.91	298.15	53.24
40	353.15	16.55	21.77	298.15	54.80
40	373.15	7.60	24.15	298.15	55.32
40	393.15	4.54	27.28	298.15	54.27
40	413.15	0.70	29.73	298.15	54.32
40	433.15	5.28	13.47	308.15	57.12
50	353.15	0.89	14.9	308.15	56.81
50	373.15	5.59	16.33	308.15	53.26
50	393.15	4.28	18.91	308.15	54.56
50	413.15	3.10	21.43	308.15	53.52
50	433.15	2.53	24.28	308.15	54.47
			26.87	308.15	55.49
			29.8	308.15	56.00

3.5 Evaluation of salt precipitation

Water diffusion coefficient in CO_2 can be used to calculate the time when precipitation occurs. Alberta Basin in Canada is a case for CO_2-H_2S saline aquifer storage (Stefan Bachu; John J. Carroll, 2005). Site 11 is used to apply the experimental data, because the P-T condition of Site 11 is similar with this study and CO_2 is the major content (82%) of the gas in this site. Pressure is 24.68 MPa and temperature is 376.15 K in this site, and water diffusion coefficient in CO_2 is 3.273×10^{-8} m^2/s. Based on the relationship between solubility (Wang et al., 2018) and concentration gradient, the concentration gradient $\frac{\frac{x_1}{(1-x_1)V_{CO_2}}-\frac{x_2}{(1-x_2)V_{CO_2}}}{\Delta l}$ in this P-T condition is $\frac{0.7197}{76.901\times10^{-6}} = 9358.79\ mol/m^4$. Diffusion flux can be obtained as:

$$J = D\frac{\partial C}{\partial l} = 3.273\times10^{-8}\times9358.79 = 3.0631\times10^{-4}\ mol/(s\cdot m^2) \quad (21)$$

For simplification, a one-dimensional pore is chosen for evaluation, and the water length is regards as 2 cm, and salt in brine is NaCl. The salinity is 2.276 mol/kg while the salt solubility in water is 6.699 mol/kg (Sawamura et al., 2007), and for salt precipitation, water is supposed to dissolve 66.0%.

Based on the calculated diffusion flux,

$$\mathrm{J}\times\mathrm{A}\times\mathrm{t} = \frac{\mathrm{A}\times2\times0.66\times0.01}{\mathrm{V}_{brine}} \quad (22)$$

$$\mathrm{t} = \frac{0.0132/(18.416\times10^{-6})}{3.0678\times10^{-4}} = 2.3364\times10^{6}s = 27\ \mathrm{day} \quad (23)$$

According to the calculation result, salt precipitation will occur 27 days after starting injecting CO_2 in to saline aquifer. Comparing with the project period, the salt precipitation occurs too early and will impair CO_2 injectivity.

3.6 Observation of salt precipitation in capillary tube

For observing the whole process of salt precipitation, small amount of high salinity solution is used for sample preparation. The length of solution in tube is 3.8 mm and the salinity is 5 mol/kg, while the experimental pressure and temperature is 20 MPa and 373.15 K. 139 hours after injecting CO_2, large amount of small crystals appears instantaneously in the solution (Fig. 7a), and crystals grows to be several large cubic crystals with evaporation (Fig. 7b-e). During growing, crystals are becoming more and more angular and the growing process takes about 43 hours after crystals appear. At the same time, the water is evaporating, and when none liquid water exists, precipitated crystals are in gas phase, and at the end of tube, crystals are irregular (Fig. 7f). According to the result, for salt precipitation, gas can only go through the pore between crystals and pipe well, and the displacement rate is weakened clearly because crystals occupy much pore pace and decreases CO_2-brine interface area.

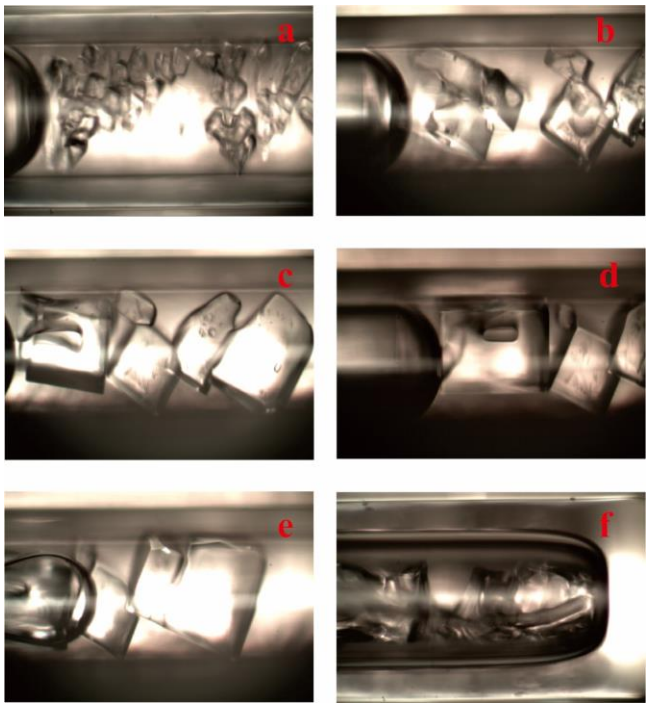

Figure 7. Pictures of salt precipitation process.

3.7 Observation of salt precipitation in micromodel

A physical rock type of micromodel is used to observe salt precipitation location in porous media. The porosity of the micromodel is 0.57. The chip is saturated with 4 mol/kg NaCl solution and is injected with pure CO_2. The temperature is 294.15±1 K and pressure is 2 MPa. When injecting CO_2 into the pore space, the displacement phenomenon is different from that in capillary tube, and at the CO_2-brine mixture zone, there does not exist a specific complete gas-liquid interface. When CO_2 starts to entry into the brine, CO_2 is surrounded by brine and then,

gas saturation becomes larger and brine is surrounded by CO_2 until all brine is dissolved or displaced.

The gas phase is the earliest precipitation zone and salt aggregates form in the gas phase and near the CO_2 interface. Salt in gas phase is a thin coat on the surface which has little influence on permeability which has little effect on CO_2 injection. During the first stage, CO_2 is surrounded by brine and salt precipitation occurs at the whole gas bubble especially at the interface. With the CO_2 and brine flowing, the salt does not move at all.

In the aqueous phase, salt precipitation is more likely to occur at the pore throat (fig.8a, b) and gas-liquid interface (fig.8d-f) which does weaken permeability and impair CO_2 injectivity. The salt moves with the flow, and when measuring the permeability after the salt precipitation, the permeability decreases more than five times mostly due to the accumulation of salt in pore throat.

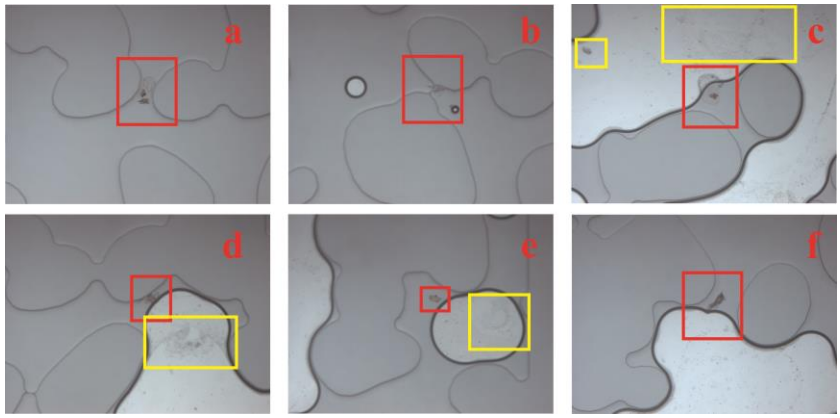

Figure 8. Salt precipitation in the micromodel. Red squares are salt in aqueous phase and yellow means salt in gas phase.

5 Conclusions

Water diffusion in CO_2 at 10-50 MPa and 353.15-433.15 K is observed by Raman quantitative spectroscopy and 22 diffusion coefficient data are obtained. Diffusion coefficient increases with temperature and reciprocal of density linearly and decreases with pressure. Based on free volume theory and PC-SAFT EOS, a thermodynamic diffusion model for water diffusion in CO_2 is established and may predict water diffusion coefficient in CO_2 accurately at 10-50 MPa and 353.15-433.15 K.

At the Alberta Basin site 11 injection well, calculated diffusion coefficient is applied to evaluate when salt precipitation occurs, and it will occur 27 days after CO_2 injection which does weaken CO_2 injectivity. Salt precipitation observation presents precipitated crystals decrease pore size dramatically and salt accumulates at the pore throat and gas-liquid interface which weaken CO_2 mass transfer obviously.

Acknowledgments, Samples, and Data

This work was supported by the National Sciences Foundation of China (No. 41472218, 41672244) and the Fundamental Research Funds for National Universities, China University of Geosciences (Wuhan). All the data for this research are included in this submitted paper.

References

Bai, B., Wu, H., & Li, X. (2018). Investigation on the relationship between wellhead injection pressure and injection rate for practical injection control in CO_2 geological storage projects. Geofluids, 2018. https://doi.org/10.1155/2018/4927415

Espinoza, D. N., & Santamarina, J. C. (2010). Water-CO_2-mineral systems: Interfacial tension, contact angle, and diffusion-Implications to CO_2 geological storage. Water Resources Research, 46(7). https://doi.org/10.1029/2009WR008634

Gaus, I. (2010). Role and impact of CO_2-rock interactions during CO_2 storage in sedimentary rocks. International Journal of Greenhouse Gas Control, 4(1), 73–89. https://doi.org/10.1016/j.ijggc.2009.09.015

Gross, J., & Sadowski, G. (2001). Perturbed-chain SAFT: An equation of state based on a perturbation theory for chain molecules. Industrial and Engineering Chemistry Research, 40(4), 1244–1260. https://doi.org/10.1021/ie0003887

Guo, H., Huang, Y., Chen, Y., & Zhou, Q. (2016). Quantitative Raman Spectroscopic Measurements of CO_2 Solubility in NaCl Solution from (273.15 to 473.15) K at p = (10.0, 20.0, 30.0, and 40.0) MPa. Journal of Chemical and Engineering Data, 61(1), 466–474. https://doi.org/10.1021/acs.jced.5b00651

Guyant, E., Han, W. S., Kim, K. Y., Park, M. H., & Kim, B. Y. (2015). Salt precipitation and CO_2 brine flow distribution under different injection well completions. International Journal of Greenhouse Gas Control, 37, 299–310. https://doi.org/10.1016/j.ijggc.2015.03.020

Han, W. S., & Mcpherson, B. J. (2009). Optimizing geologic CO_2 sequestration by injection in deep saline formations below oil reservoirs. Energy Conversion and Management, 50(10), 2570–2582. https://doi.org/10.1016/j.enconman.2009.06.008

Jeddizahed, J., & Rostami, B. (2016). Experimental investigation of injectivity alteration due to salt precipitation during CO_2 sequestration in saline aquifers. Advances in Water Resources, 96, 23–33. https://doi.org/10.1016/j.advwatres.2016.06.014

Kazimierz Krynicki, B. Y., Green, C. D., Sawyer, D. W., Krynicki, K., Green, C. D., & Sawyer, D. W. (1978). Pressure and temperature dependence of self-diffusion in water. Faraday Discuss. Chem. Soc., 66, 199. https://doi.org/10.1039/DC9786600199

Liu, H., Silva, C. M., & Macedo, E. A. (2002). Generalised free-volume theory for transport properties and new trends about the relationship between free volume and equations of state. Fluid Phase Equilibria, 202(1), 89–107. https://doi.org/10.1016/S0378-3812(02)00083-3

Lu, W., Guo, H., Chou, I. M., Burruss, R. C., & Li, L. (2013). Determination of diffusion coefficients of carbon dioxide in water between 268 and 473K in a high-pressure capillary optical cell with in situ Raman spectroscopic measurements. Geochimica et Cosmochimica Acta, 115, 183–204. https://doi.org/10.1016/j.gca.2013.04.010

Miri, R., van Noort, R., Aagaard, P., & Hellevang, H. (2015). New insights on the physics of salt precipitation during injection of CO_2 into saline aquifers. International Journal of Greenhouse Gas Control, 43, 10–21. https://doi.org/10.1016/j.ijggc.2015.10.004

Muller, N., Qi, R., Mackie, E., Pruess, K., & Blunt, M. J. (2009). CO_2 injection impairment due to halite precipitation. Energy Procedia, 1(1), 3507–3514. https://doi.org/10.1016/j.egypro.2009.02.143

Ott, H., Roels, S. M., & de Kloe, K. (2015). Salt precipitation due to supercritical gas injection: I. Capillary-driven flow in unimodal sandstone. International Journal of Greenhouse Gas Control, 43, 247–255. https://doi.org/10.1016/j.ijggc.2015.01.005

Pruess, K., & Müller, N. (2009). Formation dry-out from CO_2 injection into saline aquifers: 1. effects of solids precipitation and their mitigation. Water Resources Research, 45(3), 1–11. https://doi.org/10.1029/2008WR007101

Robb, W. L., & Drickamer, H. G. (1951). Diffusion in CO_2 up to 150-atmospheres pressure. The Journal of Chemical Physics, 19(12), 1504–1508. https://doi.org/10.1063/1.1748110

Roels, S. M., Ott, H., & Zitha, P. L. J. (2014). μ-CT analysis and numerical simulation of drying effects of CO_2 injection into brine-saturated porous media. International Journal of Greenhouse Gas Control, 27, 146–154. https://doi.org/10.1016/j.ijggc.2014.05.010

Sawamura, S., Egoshi, N., Setoguchi, Y., & Matsuo, H. (2007). Solubility of sodium chloride in water under high pressure. Fluid Phase Equilibria, 254(1–2), 158–162. https://doi.org/10.1016/j.fluid.2007.03.003

Schwertz, F. A., & Brow, J. E. (1951). Diffusivity of water vapor in some common gases. The Journal of Chemical Physics, 19(5), 640–646. https://doi.org/10.1063/1.1748306

Stefan Bachu; John J. Carroll. (2005). In-situ phase and thermodynamic properties of resident brine and acid gases (CO_2 and H_2S) injected into geological formations in western Canada. Greenhouse Gas Control Technologies, 1, 49–451.

Wang, Z., Zhou, Q., Guo, H., Yang, P., & Lu, W. (2018). Determination of water solubility in supercritical CO_2 from 313.15 to 473.15 K and from 10 to 50 MPa by in-situ quantitative Raman spectroscopy. Fluid Phase Equilibria, 476, 170–178. https://doi.org/10.1016/j.fluid.2018.08.006

Woolf, B. Y. L. A., & Dyo, T. (1974). Tracer Diffusion of Tritiated Water (THO) in Ordinary Water (H_2O) und & Pressure, 784–796.

Xu, B., Nagashima, K., DeSimone, J. M., & Johnson, C. S. (2003). Diffusion of water in liquid and supercritical carbon dioxide: An NMR study. Journal of Physical Chemistry A, 107(1), 1–3. https://doi.org/10.1021/jp021943g

Yang, X. N., Coelho, L. A. F., & Matthews, M. A. (2000). Near-critical behavior of mutual diffusion coefficients for five solutes in supercritical carbon dioxide. Industrial and Engineering Chemistry Research, 39(8), 3059–3068. https://doi.org/10.1021/ie990705d